Analytic band Monte Carlo model for electron transport in Si including acoustic and optical phonon dispersion

Eric Pop[a] and Robert W. Dutton
Department of Electrical Engineering, Stanford University, Stanford, California 94305

Kenneth E. Goodson
Department of Mechanical Engineering, Stanford University, Stanford, California 94305

We describe the implementation of a Monte Carlo model for electron transport in silicon. The model uses analytic, nonparabolic electron energy bands, which are computationally efficient and sufficiently accurate for future low-voltage (<1 V) nanoscale device applications. The electron-lattice scattering is incorporated using an isotropic, analytic phonon-dispersion model, which distinguishes between the optical/acoustic and the longitudinal/transverse phonon branches. We show that this approach avoids introducing unphysical thresholds in the electron distribution function, and that it has further applications in computing detailed phonon generation spectra from Joule heating. A set of deformation potentials for electron-phonon scattering is introduced and shown to yield accurate transport simulations in bulk silicon across a wide range of electric fields and temperatures. The shear deformation potential is empirically determined at $\Xi_u=6.8$ eV, and consequently, the isotropically averaged scattering potentials with longitudinal and transverse acoustic phonons are $D_{LA}=6.39$ eV and $D_{TA}=3.01$ eV, respectively, in reasonable agreement with previous studies. The room-temperature electron mobility in strained silicon is also computed and shown to be in better agreement with the most recent phonon-limited data available. As a result, we find that electron coupling with g-type phonons is about 40% lower, and the coupling with f-type phonons is almost twice as strong as previously reported. © *2004 American Institute of Physics.*
[DOI: 10.1063/1.1788838]

I. INTRODUCTION

The Monte Carlo (MC) method is regarded as the most comprehensive approach for simulating charge transport in semiconductors. An early standard was set by the work of Canali *et al.*[1] and Jacoboni and Reggiani[2] using analytic, ellipsoidal descriptions of the energy-band structure. Over the past two decades, the research community has added numerous enhancements, including more comprehensive physical models, more efficient computer algorithms, new scattering mechanisms, boundary conditions, electrostatic self-consistency in device simulations, etc. A significant enhancement of the physical models was the introduction of full electron energy bands from empirical pseudopotential calculations.[3,4]

For device operating voltages near 5 V, the full band MC method has been very useful with high-energy transport simulations, including impact ionization,[3,5] where details of the full band structure are essential. As device dimensions are scaled into the nanometer range and supply voltages are reduced below the material's band gap (1.1 V for silicon), the role of impact ionization is greatly diminished. Transport at lower energies can be adequately simulated with analytic band models. Hence, simpler, faster analytic band MC codes (including quantum mechanical corrections where required by confined dimensions) can be employed as engineering design tools for future nanoscale devices. In addition, despite the increasing sophisticated treatment of the electron energy bands over the years, the phonon dispersion relation is still commonly simplified in practical device simulators. The electron-phonon scattering is usually computed with a single dispersionless acoustic mode and with one (or a few) fixed-energy optical modes. This paper presents a MC model which uses complete analytical descriptions for both the electron band structure and the phonon dispersion relationship. The approach is computationally efficient on modern desktop workstations and suitable for simulating electron transport in future, low-voltage technologies, while describing the electrons and phonons with comparable accuracy.

Figure 1 shows a brief historical overview of various MC simulation methods for charge transport in silicon.
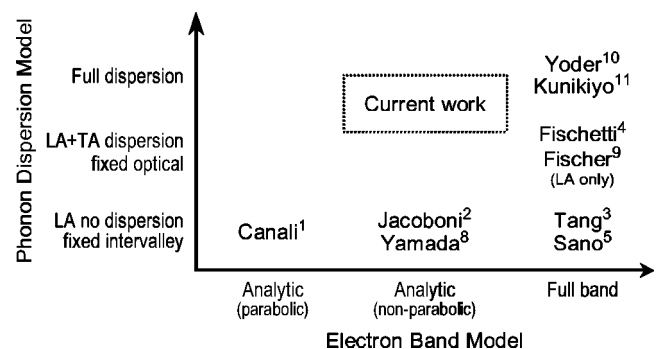
FIG. 1. Historical context of various Monte Carlo models for electron transport in silicon. The computational burden increases for full band (and full dispersion) simulations.

a)Electronic address: epop@alum.mit.edu

Canali et al.[1] introduced the first multivalley model with parabolic, ellipsoidal bands and phonon scattering with a single dispersionless longitudinal acoustic (LA) mode and six fixed-energy intervalley phonons. Jacoboni et al.[6] accounted for analytic band nonparabolicity and slightly altered Canali's set of phonon deformation potentials. A few years later, Brunetti et al.[7] introduced a new set of deformation potentials, more closely matching available data on the anisotropy of electron diffusion in silicon. This phonon model was used by Jacoboni et al.[6] in an excellent and frequently referenced review of the MC method,[2] and it subsequently became the set of phonon energies and deformation potentials most often employed in the literature over the past two decades. Yamada et al.[8] also introduced scattering with the first-order intervalley phonons. Tang and Hess[3] were the first to incorporate the full band structure of silicon (computed from empirical pseudopotentials) for MC transport. However, they used the simple phonon model of Canali/Brunetti (dispersionless LA phonons, six fixed-energy intervalley phonons) and the deformation potentials of Brunetti et al.[7] Sano et al. introduced the wave vector-dependent impact ionization rates in a full band MC formulation[5] but computed the phonon scattering rates with the multivalley deformation potentials of Canali et al.[1]

Realistic device simulations using electrostatically self-consistent full band MC were first performed by Fischetti and Laux.[4] They were also the first to make the distinction between longitudinal (LA) and transverse acoustic (TA) intravalley scattering using a simple analytic dispersion for both modes. Fischer and Hofmann[9] pointed out the poor definition of energy "valleys" in the context of full band models and used only two averaged deformation potentials: one for the fixed-energy optical phonons and another for the acoustic phonons (LA, but not TA), including their dispersion. The most sophisticated MC models for the charge transport in silicon were developed by Yoder and Hess[10] and Kunikiyo et al.[11] They employed the full band structure computed from empirical pseudopotentials and the full (anisotropic) phonon dispersion obtained from an adiabatic bond-charge model. The electron-phonon scattering rates were calculated as a function of energy and wave vector, consistently with the band structure and the phonon dispersion. In the absence of any adjustable parameters, mobilities computed with these *ab initio* models are typically less accurate than those computed using more empirical simulators. Such codes also present formidable computational burdens, rendering them impractical for simulations of realistic devices. Their only applications have been for very detailed bulk transport calculations.

Most MC codes found in practice today employ a sophisticated, full description of the electron energy bands (often including quantum effects[12]), yet scattering rates and energy exchange with the lattice are only computed with a simplified phonon dispersion.[13,14] The phonon energies and the deformation potentials most often used are those originally introduced by Brunetti et al.[7] Optical phonon dispersion is ignored and often only one acoustic branch (LA) is considered for intravalley scattering. Such models can lead to unphysical thresholds in the electron distribution function[9]

and cannot be used to compute phonon generation rates for detailed phonon dynamics simulations (e.g., phonon Boltzmann transport or molecular dynamics). In a realistic electron device, a full phonon dispersion is essential for extracting the correct phonon generation spectrum from Joule heating.[15]

In what follows, we describe the implementation of a MC code which uses analytic descriptions for both the electron bands and the phonon dispersion. In the context of Fig. 1, the current isotropic analytic phonon model lies on the vertical axis between the anisotropic bond-charge dispersion method[10,11] and all the other traditional approaches. This computationally efficient method is suitable for simulating low-voltage nanodevices, while treating the electron bands and the phonon dispersion with equal attention.

II. IMPLEMENTATION

The general aspects of the Monte Carlo method for charge transport in semiconductors have been well described before.[2,16,17] In brief, the ensemble MC approach used in this work preselects several tens of thousands "superparticles" to represent the mobile charge inside the semiconductor. This number is limited by computational and memory constraints, but good statistics can be obtained if the simulation is run for an adequately long time. The particles are initialized with thermal energy distributions or based on the initial conditions read from, for example, a drift-diffusion device simulator. The superparticles are treated as single carriers during their free flights and as charge clouds when the Poisson equation is solved. A fictive "self-scattering" rate can be chosen in such a way that the sum of all scattering rates is constant and independent of the carrier energy. The distribution of free flight times is directly related to this total scattering rate.[16] For each particle, a random number is drawn to determine its time of free flight. During this time, the carrier is allowed to drift under the influence of the electric field. Then, another random number[18] is drawn and compared with cumulative probabilities of scattering, which have been precomputed as a function of energy. A scattering mechanism (e.g., with impurities, acoustic or optical phonons) is selected in proportion to the strength of each process. If self-scattering is selected, the particle continues its free flight unimpeded. If a real scattering process is selected, the particle's energy and momentum are adjusted as necessary and another random time of flight is drawn. This procedure then repeats for all particles. Statistics are gathered by sampling the superparticle system at regular time intervals, until the targeted accuracy is reached. The error margins are inversely proportional to the square root of the number of superparticles being simulated.

A. Electron Band Model

This work models the electron energy bands analytically, following Jacoboni and Reggiani[2] and including the nonparabolicity parameter α (=0.5 eV^{-1} at room temperature). With $\alpha=0$ the kinetic energy is purely parabolic and the original model of Canali et al.[1] is recovered. All six ellipsoidal, energetically equivalent conduction-band valleys of sili-
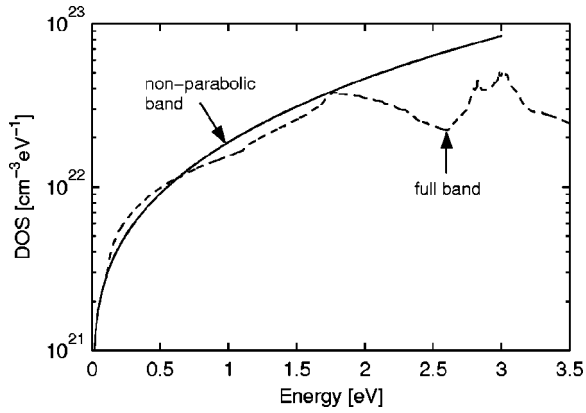
FIG. 2. Conduction-band density of states (DOS) in Si from a full band calculation (courtesy C. Jungemann) vs. the DOS computed with the non-parabolic band approximation.
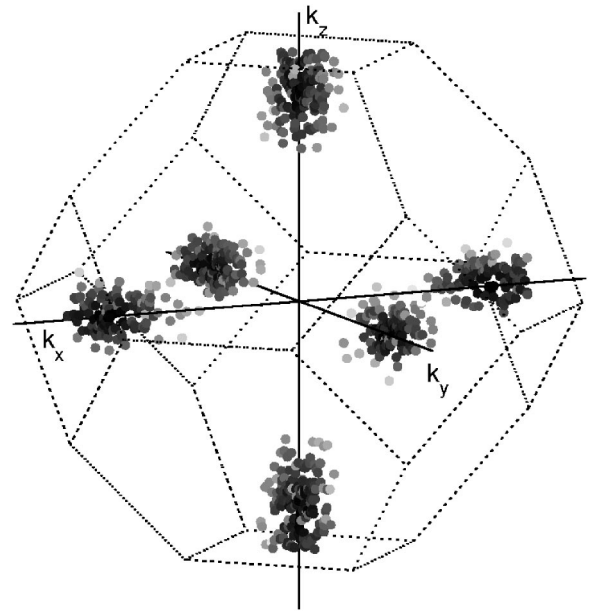

FIG. 3. Electron distribution in momentum space, for an electric field of 50 kV/cm in the (111) direction, at 300 K. Higher energy electrons are shown with lighter shades of gray.

con are explicitly included. The nonparabolic band approximation represents a good description of electron transport at energies below approximately 1 eV, such as those of future low-voltage nanotechnologies, where impact ionization and high-energy transport are not expected to play a significant role. Figure 2 shows a comparison between the total conduction-band density of states (DOS) computed in the nonparabolic band approximation and the full band density of states. The relationship between the electron energy E_k and the wave vectors k_i ($i=1$, 2 or 3, for the three Cartesian axes) is

$$E_k(1 + \alpha E_k) = \frac{\hbar^2}{2} \sum_{i=1}^{3} \frac{(k_i - \kappa_{vi})^2}{m_i}, \quad (1)$$

where m_i is the component of the electron mass tensor along the ith direction and κ_{vi} represents the coordinates of the respective conduction-band minimum. Silicon has six equivalent conduction-band minima near the X symmetry points, located at ± 0.85 of the distance from the middle to the edge of the Brillouin zone, along the three axes. For example, the X valley along the (100) direction is centered at $(0.85,0,0)G$, where $|\mathbf{G}|=2\pi/a$ is the reciprocal lattice vector and $a=5.431$ Å is the silicon lattice constant. The mass tensor components are the longitudinal mass $m_l/m_0=0.916$ and the transverse mass $m_t/m_0=0.196$ at room temperature, where m_0 is the mass of the free electron. We also include the temperature dependence of the band gap $E_G(T)$ analytically, following the review of Green.[19] This dictates a slight temperature dependence of the transverse mass as $m_t/m_0=0.196 E_{G0}/E_G(T)$ and of the nonparabolicity parameter as $\alpha=0.5 E_{G0}/E_G(T)$ eV^{-1}, where E_{G0} is the silicon band gap at room temperature.[19] Figure 3 shows a typical "snapshot" of the electron distribution in momentum space, as represented by the current work. Electrons that exit the first Brillouin zone (drawn with dotted lines in Fig. 3) are reflected back into the opposite conduction-band valley.

Since it uses the analytic nonparabolic band approximation, suitable for low-energy studies, the present work ignores the second conduction band (the L valley) of silicon, which lies slightly more than 1 eV above the bottom of the X valley. Hence, the maximum electron energy is usually lim-

ited to 1 eV during the simulation. In fact, this upper limit on the electron energy is a convenient value for several reasons: (a) it is the approximate energy difference between the L and the X valleys, (b) it is also about the value of the silicon energy band gap, which controls impact ionization, and (c) it conveniently corresponds to an upper limit on the maximum electron energy in low-voltage future nanodevices, which will operate at 1 V or below. Since electrons with energies larger than the band gap will be rare, impact ionization is not expected to play a significant role and consequently, it can be safely neglected.

B. Phonon Scattering Model

The present work treats all phonon scattering events inelastically, hence, the electrons exchange the correct amount of energy (corresponding to the absorption or emission of a phonon) with each scattering event. Particular attention is paid to the treatment of inelastic acoustic phonon scattering to properly account for energy dissipation at low temperatures and low electric fields. Treating the acoustic phonons inelastically is also important for heat generation spectrum calculations.[15] Figure 3 and the inset of Fig. 4 illustrate the ellipsoidal conduction-band valleys and the allowed phonon scattering transitions. As in the traditional analytic-band approach,[2] scattering with six types of intervalley phonons is incorporated. Intervalley scattering can be of g type, when electrons scatter between valleys on the same axis, e.g., from (100) to (-100), or of f type when the scattering occurs between valleys on perpendicular axes, e.g., from (100) to (010).[20] Intravalley scattering refers to scattering within the same conduction-band valley and usually involves only acoustic phonons.[21]

Most typical MC codes,[2,5–9] both analytic- and full-band, treat intravalley scattering with a single kind of acoustic phonon. This simplification is accomplished by grouping the
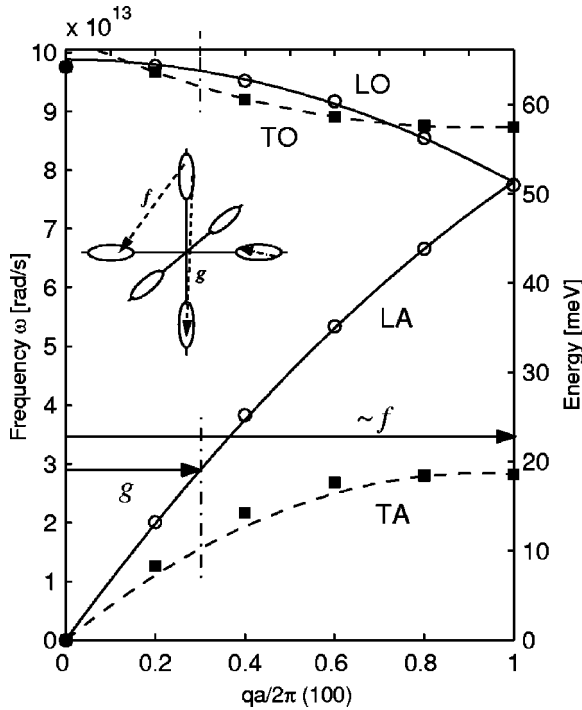
FIG. 4. Phonon dispersion in silicon along the (100) direction, from neutron scattering data (symbols). (see Ref. 37) The lines represent our quadratic approximation. The f and g phonons participate in the intervalley scattering of electrons (See Ref. 20).

longitudinal acoustic (LA) and the transverse acoustic (TA) branches into a dispersionless mode with a single velocity and a single deformation potential. Unlike the traditional approach, this work considers scattering with LA and TA modes separately. Each phonon dispersion branch from Fig. 4 (including the optical modes) is treated with the isotropic approximation

$$\omega_q = \omega_o + v_s q + cq^2, \tag{2}$$

where ω_q is the phonon frequency and q is the wave vector. For acoustic phonons, the parameters v_s and c can be chosen to capture the slope of the dispersion near the Brillouin zone center and the maximum frequency at the zone edge, similar to Ref. 9. The choice of parameters for longitudinal optical (LO) phonons insures that they meet the zone edge LA frequency. For both the TA and transverse optical (TO) phonons, the zone edge slope, i.e., their group velocity is fit to zero. The continuous (longitudinal) and dashed (transverse) lines in Fig. 4 represent these quadratic approximations, and the fitting coefficients are listed in Table I. Quartic polynomials would offer a better fit in the (100) crystal direction but no advantage in the other directions, hence, the

TABLE I. Quadratic phonon dispersion coefficients.

	ω_o 10^{13} rad/s	v_s 10^5 cm/s	c 10^{-3} cm^2/s
LA	0.00	9.01	−2.00
TA	0.00	5.23	−2.26
LO	9.88	0.00	−1.60
TO	10.20	−2.57	1.11

quadratics are entirely sufficient for this isotropic approximation. They track the phonon dispersion data closely, especially in the regions relevant to electron-phonon scattering in silicon: near the Brillouin zone center for long wavelength intravalley acoustic phonons and near the frequencies corresponding to intervalley f- and g-type phonons. The quadratics are also easy to invert and, where needed, to extract the phonon wave vector as a function of frequency.

The same approach can be used to extend this phonon dispersion model to other materials or confined dimensions. Changes in the phonon dispersion due to a strain or confinement (e.g., in nanostructures) can be easily included. The challenge in this case lies chiefly in determining the correct modified phonon dispersion to use in such circumstances. The electron-phonon scattering rates need to be numerically recomputed with the modified phonon description (as outlined below), which can be done efficiently if the dispersion is written as a set of analytic functions, like the polynomials in this paper.

C. Intravalley Scattering

The total intravalley scattering rate is calculated separately with the LA and TA phonons, as a function of the initial electron energy E_k

$$\Gamma_i(E_k) = \frac{D_a^2 m_d}{4\pi\rho\hbar^2 k_s} \int_q \frac{1}{\omega_q}\left(N_q + \frac{1}{2} \mp \frac{1}{2}\right)\mathcal{I}_q^2 q^3 dq, \tag{3}$$

where D_a is the respective deformation potential (D_{LA} or D_{TA}), $m_d = (m_t^2 m_l)^{1/3}$ is the electron density of states effective mass, and ρ is the mass density of silicon. The top and the bottom signs refer to phonon absorption and emission, respectively. The electron wave vector is transformed to spherical Herring-Vogt[22] space as

$$k_s = \sqrt{2m_d E_k(1 + \alpha E_k)}/\hbar. \tag{4}$$

Since the scattering rates are numerically integrated at the beginning of the simulation, the correct phonon occupation can be incorporated, $N_q = 1/(\exp(\hbar\omega_q/k_B T) - 1)$, without resorting to the equipartition or Joyce-Dixon approximations normally used.[2] The wave function overlap integral is included in the rigid ion approximation[23]

$$\mathcal{I}_q = \frac{3}{(qR_s)^3}[\sin(qR_s) - qR_s\cos(qR_s)], \tag{5}$$

where $R_s = a[3/(16\pi)]^{1/3}$ is the radius of the spherical Wigner-Seitz cell, $R_s = 2.122$ Å for silicon. All quantities are numerically evaluated using the corresponding phonon dispersion. The scattering rate integral in Eq. (3) is carried out over all phonon wave vectors that conserve both energy ($E_k' = E_k \pm \hbar\omega_q$) and momentum ($\mathbf{k}' = \mathbf{k} \pm \mathbf{q}$). These arguments can be used to establish the range of q, as required by $|\cos(\phi)| \leq 1$, where

$$\cos(\phi) = \mp\frac{q}{2k_s} + \frac{m_d\omega_q}{\hbar q k_s}[1 + \alpha(2E_k \pm \hbar\omega_q)] \tag{6}$$

and ϕ is the angle between the phonon and initial electron wave vector. As in the rest of this paper, the top and the

TABLE II. Summary of intervalley phonon energies and deformation potentials for electrons in silicon.

	Type	T(K)	E(meV)	Deformation potentials $\Delta_{if}(10^8$ eV/cm)				
				Canali *et al.* (Ref. 1)	Joergensen (Ref. 36)	Brunetti *et al.* (Ref. 7)	Yamada *et al.* (Ref. 8)	This work
f_1	TA	220	19	0.15	—	0.3	2.5	0.5
f_2	LA/LO	550	51	3.4	4.3	2	—	3.5
f_3	TO	685	57	4	2	2	8	1.5
g_1	TA	140	10	0.5	0.65	0.5	—	0.3
g_2	LA	215	19	0.8	—	0.8	4	1.5
g_3	LO	720	62	3	7.5	11	8	6

bottom signs refer to phonon absorption and emission, respectively. The intravalley scattering rate typically cited in the literature[2] can be recovered by substituting $\omega_q = v_s q$, $\mathcal{I}_q = 1$ and using an approximation for N_q, which allows Eq. (3) to be integrated analytically.

The final state of the electron after scattering $(E'_k, \mathbf{k}')$ reflects both the energy and momentum exchange with the phonon, as follows: first, the value of q is selected within the allowed range using a rejection algorithm[2] applied to the integrand in Eq. (3), which includes the overlap integral. Then the magnitude of the electron wave vector $\mathbf{k}'$ after scattering is found by energy conservation, whereas the angle between $\mathbf{k}'$ and $\mathbf{k}$ is obtained by momentum conservation. The final electron state is only accepted if it falls within the first Brillouin zone, otherwise, the rejection algorithm is repeated.

The intravalley deformation potentials have a general angular dependence, which can be written as[22]

$$\Xi_{LA}(\theta) = \Xi_d + \Xi_u \cos^2 \theta, \qquad (7)$$

$$\Xi_{TA}(\theta) = \Xi_u \sin \theta \cos \theta, \qquad (8)$$

where θ is the angle between the phonon wave vector and the longitudinal axis of the conduction-band valley, Ξ_u is the shear, and Ξ_d is the dilation deformation potential. Detailed calculations have shown that the influence of this angular dependence on the electron transport is relatively small.[24] Hence, the intravalley deformation potentials can be averaged over the angle θ, consistently with the general isotropic approach adopted in this work. The isotropically averaged deformation potentials become

$$D_{LA} = \sqrt{\frac{\pi}{2}\left(\Xi_d^2 + \Xi_d\Xi_u + \frac{3}{8}\Xi_u^2\right)}, \qquad (9)$$

$$D_{TA} = \frac{\sqrt{\pi}}{4}\Xi_u, \qquad (10)$$

which are used for computing the intravalley scattering rates in Eq. (3). There is considerable variation in the values of the shear (Ξ_u) and dilation (Ξ_d) deformation potentials reported in the literature over the years. A good summary of these values can be found in Ref. 25: various theoretical and empirical studies have estimated Ξ_u in the range from 7.3 to 10.5 eV, whereas Ξ_d has been previously cited both as -11.7 eV (Ref. 26) and near 1.1 eV (Ref. 25). Although, perhaps surprisingly, both values can be used to describe

electron mobility (hence, the original confusion over the correct choice), it was shown that only the latter ($\Xi_d = 1.1$ eV) yields the correct mobilities both for electrons and holes.[25] This is the value adopted in the current study. We then use Ξ_u as a fitting parameter, while calculating the low-field, low-temperature (T=77 K) electron mobility, a regime dominated by scattering with intravalley phonons. An empirical best-fit value of $\Xi_u = 6.8$ eV is found, in reasonable agreement with previous work. With these values of Ξ_d and Ξ_u, the isotropically averaged deformation potentials are $D_{LA} = 6.39$ eV and $D_{TA} = 3.01$ eV. These are comparable with the value of 9 eV typically cited in the literature for MC models where scattering is only taken into account with the longitudinal modes.[2]

D. Intervalley Scattering

As outlined in Sec. II B, intervalley scattering in silicon can take electrons between the equivalent (*g*-type) and nonequivalent (*f*-type) valleys. Based on geometrical arguments,[20] both the *f*- and *g*-type scattering are Umklapp processes involving a reciprocal lattice vector $|\mathbf{G}| = 2\pi/a$. Since the *X*-valley minima are located at 0.85 from the center to the edge of the Brillouin zone, the change required in electron momentum is $(0, 0.85, 0.85)G$ for *f*-type scattering and $(1.7, 0, 0)G$ for *g*-type scattering. Reduced to the first Brillouin zone, the phonons involved are $(1, 0.15, 0.15)G$ and $(0.3, 0, 0)G$, respectively.[27] The *f* phonon is just 11° off the (100) direction, whereas the *g* phonon is along (100) at $0.3G$. These phonons are schematically drawn on the dispersion relation in Fig. 4. The *g*-phonon frequencies can be directly read off the (100) dispersion, whereas the *f* phonons are typically assumed to be those at the edge of the Brillouin zone. In this work, ω_q is computed from the analytic phonon dispersion, and the intervalley scattering rate can be written as follows:[2,16]

$$\Gamma_{if}(E_k) = \frac{\pi\Delta_{if}^2 Z_f}{2\rho\omega_q}\left(N_q + \frac{1}{2} \mp \frac{1}{2}\right)g_{df}(E_k \pm \hbar\omega_q), \qquad (11)$$

where Z_f is the number of available final valleys (4 for *f*-type and 1 for *g*-type scattering), $g_{df}(E)$ is the density of states in the final valley, and the other symbols are the same as previously defined. Intervalley scattering can also include an overlap factor, but its value is typically incorporated into the scattering constant Δ_{if}. The six phonons involved in intervalley scattering, along with their approximate energies, equiva-
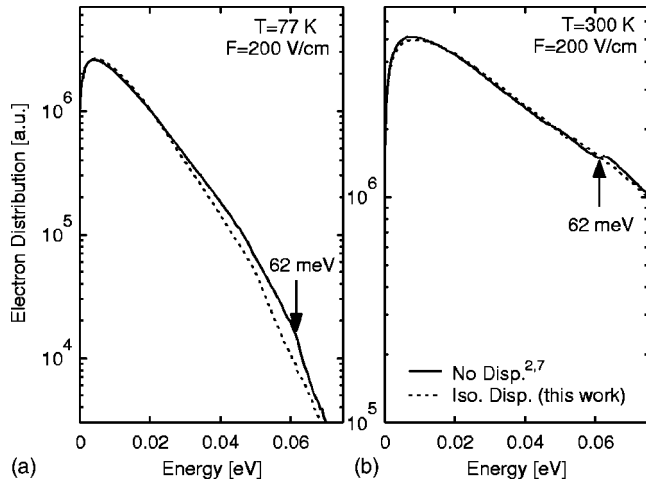
FIG. 5. Electron distribution vs. energy at (a) 77 K and (b) 300 K with low applied electric field (200 V/cm). The typical dispersionless model (See Refs. 2 and 7) is compared with the results of this work, which include the full isotropic dispersion. Note the vertical axes are not at the same scale.
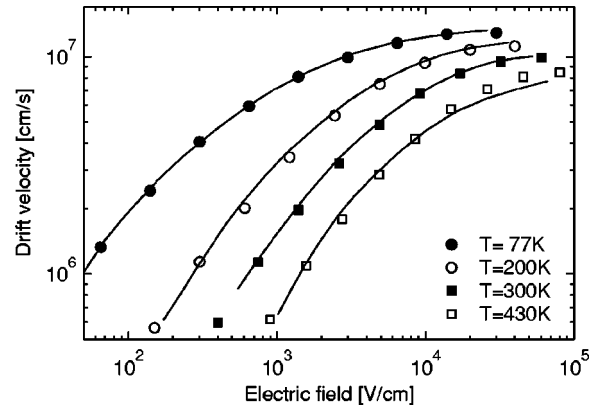

FIG. 6. Electron drift velocity vs. electric field in unstrained silicon over a wide range of temperatures. Symbols are the Monte Carlo simulations of this work. The lines represent the time of flight experimental data of Canali (see Ref. 1).

lent temperatures (as $T = \hbar \omega_q / k_B$), and deformation potential scattering constants are listed in Table II.

Traditional MC models (apart from the *ab initio* approaches of Refs. 10 and 11) assume that the phonon energies involved in intervalley scattering are fixed at the values determined by transitions between the *X*-valley minima. Also, the state of the electron in the final valley is computed isotropically.[2] These geometrical arguments only hold strictly for the lowest energy electrons at the bottom of the bands. This work takes into account the phonon dispersion for scattering with both the optical and acoustic phonons when calculating the final state of the electron. After the type of intervalley scattering mechanism is determined, the state of the electron in the final valley is first chosen isotropically, as in the traditional approach. The phonon wave vector necessary for this transition can be calculated as $\mathbf{q} = \mathbf{k}' - \mathbf{k}$, because the initial state of the electron is known. The phonon is then reduced to the first Brillouin zone and its energy is obtained using the phonon dispersion described earlier. This procedure is applied to both the acoustic and optical phonons. The phonons that do not satisfy both the energy and momentum conservation within a certain tolerance are discarded with a rejection algorithm. This is a relatively inexpensive search that ends when a suitable phonon is found. The effect of this algorithm is to smear out any "hard" thresholds associated with intervalley phonon energies in the electron distribution. Figure 5 shows the low-field (200 V/cm) electron distribution computed with this approach, compared to the typical models found in the literature,[2,7] where the intervalley phonon dispersion is not taken into account. Any unphysical threshold, e.g., at 62 meV due to *g*-type optical intervalley scattering, is removed when phonons of varying energies around this value (as given by the dispersion relation and by energy and momentum conservation) are allowed to participate. Such thresholds in the electron distribution are also present in full band MC models, which use a single, fixed-energy optical phonon.[9] The current model removes them in a computationally inexpensive way, while satisfying the energy and mo-

mentum conservation for all scattering events.

Despite the added complexity of the full phonon dispersion, this analytic band code is more than an order of magnitude faster when compared to typical full band programs (using a simpler phonon description) doing the same velocity-field curve calculations, i.e., Fig. 6. A version of the code compiled using fixed phonon energy values and without the dispersion information (essentially identical to the one of Ref. 2) was only a few percent faster than our model, which includes the dispersion. Hence, this work incorporates the phonon dispersion in an efficient way, giving significantly more physical insight than the typical analytic band code for very little computational overhead, while still being more than an order of magnitude faster than a typical full band code. The analytic phonon dispersion and the analytic electron bands significantly speed up the calculations of the final electron state after scattering, compared to the look-up tables and interpolation schemes found in full band codes. Further speed improvements can be obtained by including an energy-dependent total scattering rate,[28] which would significantly reduce the number of self-scattering events.

III. APPLICATIONS

The electron transport characteristics at moderate to high fields and for all but the lowest temperatures are determined by the choice of intervalley coupling constants Δ_{if}. This choice also determines the relative strength of the *f*- and *g*-type intervalley scattering. Several sets of coupling constants previously proposed are listed in Table II. The parameter set introduced by Brunetti *et al.*[7] has been the most commonly used in the literature over the past two decades, for both analytic and full band simulations. This parameter set strongly favors *g*-type scattering with the 62 meV LO phonon, whereas the original set of Canali *et al.*[1] tends to favor *f*-type scattering with zone edge phonons. It should be noted that the zone edge *f* phonon at 51 meV is typically classified as part of the LA branch, but this scattering can also happen with LO phonons,[24] because the two branches meet at the zone boundary. Since the current work takes into account both the acoustic and optical dispersion, when this

f-type scattering event is selected, the participating phonon is assigned to the LO branch if $|\mathbf{k}' - \mathbf{k}| > 2\pi/a$, and to the LA branch otherwise.

A. Bulk Si Mobility

The intervalley scattering constants for the current model are derived starting from the set of Brunetti *et al.*[7] To aid with parameter extraction, an inverse modeling code originally developed for doping profile extraction was modified and used.[29] The intervalley scattering parameters were extracted over a wide range of temperatures and electric fields, by comparison with the available transport data.[1,19] Low energy phonons typically control the low-field and low-temperature mobility. Increased coupling constants with low energy phonons lead to lower drift velocities and lower electron energies, both in the low-field (linear) and the high-field (saturation) region. The effect is the same in the low-field region when increasing the high-energy (optical or *f*-type LA) coupling constants. On the other hand, increased coupling constants with high-energy phonons lead to higher drift velocities in the high field region, while the average energy decreases. In other words, cooling the electron distribution through high energy phonon emission leads to higher velocities, because at higher energies, the electron velocity is curtailed by nonparabolicity, which increases the effective mass by a factor of $(1 + 2\alpha E_k)$. The low and high-energy intervalley coupling constants have the same effect on the drift velocity at low fields, but opposing effects at high fields. This opposite dependence of the velocity on low and high-energy intervalley phonons determines the "shape" of the velocity-field curves (see Fig. 6) and can be used to fine-tune the coupling constants. Since phonons involved in intervalley scattering have different energies, the inverse modeling method can distinguish between the contribution of the various parameters to the velocity-field curves. Most notably, a smaller contribution of the *g*-type LO phonon is found with a deformation potential approximately 40% lower than the value reported by Brunetti *et al.*[7] (see Table II). For the *f*-type scattering, the deformation potential of LA/LO is found to be stronger than that of TO phonons, which is consistent with *ab initio* calculations.[24]

The temperature dependence of the low-field mobility can be used to fine-tune the low energy intervalley phonon parameters, assuming that impurity scattering can be neglected. Figures 6 and 7 show the results of the transport simulations using the current set of parameters, which are listed in Table II. Note the wide range of electric fields and temperatures (from 30 K to 600 K) covered by the simulations and their comparison with the transport data. The current model agrees with this data well within the experimental error.

B. Strained Si Mobility

Strained silicon transport data was not available when the original sets of intervalley coupling constants listed in Table II were proposed. As the technology for growing defect-free strained silicon layers on top of $Si_{1-x}Ge_x$ buffers was perfected, record mobilities have been measured. Elec-
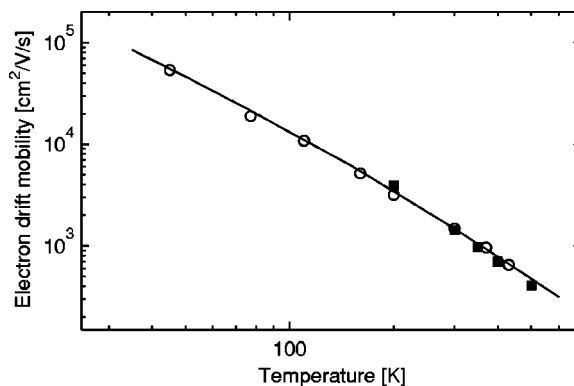

FIG. 7. Electron drift mobility simulation and data over a wide range of temperatures. Open symbols are data from Canali, (see Ref. 1) closed symbols are data from Green (see Ref. 19). The solid line was simulated with the current Monte Carlo method.

tron drift mobilities near 3000 cm²/Vs at room temperature have been reported in strained silicon modulation-doped structures (MODFETs).[30,31] These mobilities are phonon limited at room temperature, because remote impurity scattering only plays a role at much lower temperatures. Also, the lattice-matched strained silicon layer guarantees a lack of surface roughness scattering on both its sides, unlike in strained metal-oxide-semiconductor (MOS) inversion layers, where surface scattering with the oxide interface dominates. It is this lack of direct impurity scattering and of interface scattering that makes such modulation-doped structures ideal for exploring phonon scattering in strained silicon. The high mobilities observed in such MODFETs cannot be explained with the intervalley scattering parameters of Ref. 7, as they require a stronger *f*-type intervalley coupling.[25]

Incorporating strained silicon in the MC simulation is relatively straightforward. The biaxial strain removes the degeneracy of the conduction band, lifting four of the six *X* valleys by $\Delta E \simeq 0.67x$, where *x* is the Ge fraction in the $Si_{1-x}Ge_x$ buffer substrate.[8] The in-plane conductivity effective mass of the two lower valleys is the lighter transverse mass m_t of silicon. The difference in energy between the nonequivalent valleys also means that *f*-type intervalley scattering is strongly reduced as the fraction *x* increases. For $x > 0.15$, the energy splitting is large enough to almost completely suppress *f*-type scattering between the lower and the upper valleys at room temperature, and the strained silicon mobility enhancement is dominated by conduction via the two lower valleys with the lighter transverse mass. This explains the apparent "saturation" of the mobility for values of $x > 0.15$ in Fig. 8. It should be noted that the transverse electron mass is slightly increased by the presence of strain,[32] e.g., $m_t = 0.199m_0$ at $x = 0.3$, and this is taken into consideration in the current model. The mobility enhancement of the strained compared to that of the unstrained silicon is illustrated in Fig. 8. The "usual" parameter set[7] cannot account for the mobility enhancement observed experimentally. The strained mobility data suggests a stronger coupling with the *f* phonons, and consequently a weaker *g*-phonon coupling. This, along with the fine tuning explained earlier, ultimately narrows down our choice of parameter sets to that listed in the last column of Table II, which was used to generate all
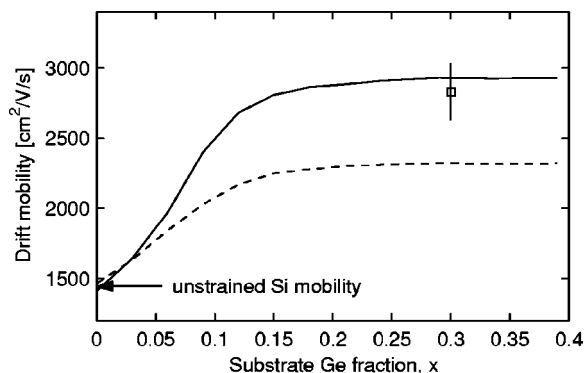
FIG. 8. Room-temperature electron mobility in strained silicon grown on $Si_{1-x}Ge_x$. Mobilities computed with this model (solid line), with the parameter set of Ref. 7 (dashed line) and the record phonon-limited mobility data from Ismail, Nelson and co-workers (see Refs. 30 and 31).

the figures. The current choice of intervalley parameters is also in close agreement with recently reported deformation potentials[21] from comprehensive theoretical calculations.[33]

IV. CONCLUSIONS

This work represents a simulation approach that fills the gap of computational tools between simple analytic-band MC codes[2,8] and more complex full-band simulators.[4,11] The emphasis is on sophisticated physical modeling within a computationally efficient framework. The use of the analytical electron bands and the phonon dispersion enables simulations that are more than an order of magnitude faster than full-band techniques, and very accessible on modern desktop computers. This method can be applied to the engineering of low-voltage nanodevices and materials that require detailed knowledge of electron-phonon coupling. The generated phonon distributions can be extracted[15] and used as inputs to a phonon transport solver.[34]

An empirically fine-tuned set of deformation potentials for intervalley scattering was introduced, which enables more accurate electron transport simulations in both strained and unstrained silicon. This work represents a different approach to analytic-band MC codes, because it distinguishes between intravalley scattering with LA and TA phonons and includes an analytic dispersion for all the phonon modes. The work can be extended beyond silicon to other materials (like germanium) or to strained or confined nanostructures. Hole transport can be simulated by modeling the valence bands like in Ref. 2 and including the full phonon dispersion.

Ongoing work is exploring the extension of these simulations to confined (and quantized) two-dimensional electron and phonon systems (e.g., ultrathin films) and to coupled electrothermal simulations. The information, documentation, and source code will be shared online.[35]

[1] C. Canali, C. Jacoboni, F. Nava, G. Ottaviani, and A. Alberigi-Quaranta, Phys. Rev. B **12**, 2265 (1975).
[2] C. Jacoboni and L. Reggiani Rev. Mod. Phys. **55**, 645 (1983).
[3] J. Y. Tang and K. Hess, J. Appl. Phys. **54**, 5139 (1983).
[4] M. V. Fischetti and S. E. Laux, Phys. Rev. B **38**, 9721 (1988).
[5] N. Sano, T. Aoki, M. Tomizawa, and A. Yoshii, Phys. Rev. B **41**, 12122 (1990).
[6] C. Jacoboni, R. Minder, and G. Maini, J. Phys. Chem. Solids **36**, 1129 (1975).
[7] R. Brunetti, C. Jacoboni, F. Nava, and L. Reggiani, J. Appl. Phys. **52**, 6713 (1981).
[8] T. Yamada, J.-R. Zhou, H. Miyata, and D. K. Ferry, IEEE Trans. Electron Devices **41**, 1513 (1994).
[9] B. Fischer and K. R. Hofmann, Appl. Phys. Lett. **76**, 583 (2000).
[10] P. D. Yoder and K. Hess, Semicond. Sci. Technol. **9**, 852 (1994).
[11] T. Kunikiyo, M. Takenaka, Y. Kamakura, M. Yamaji, H. Mizuno, M. Morifuji, K. Taniguchi, and C. Hamaguchi, J. Appl. Phys. **75**, 297 (1994).
[12] B. Winstead and U. Ravaioli, IEEE Trans. Electron Devices **50**, 440 (2003).
[13] A. Duncan, U. Ravaioli, and J. Jakumeit, IEEE Trans. Electron Devices **45**, 867 (1998).
[14] F. M. Bufler, Y. Asahi, H. Yoshimura, C. Zechner, A. Schenk, and W. Fichtner, IEEE Trans. Electron Devices **50**, 418 (2003)
[15] E. Pop, R. W. Dutton, and K. E. Goodson, in Simulation of Semiconductor Processes and Devices (Boston, MA, 2003), pp. 121–124.
[16] M. Lundstrom, *Fundamentals of carrier transport*, 2nd ed. (Cambridge University Press, Cambridge, 2000).
[17] K. Tomizawa, *Numerical simulation of submicron semiconductor devices* (Artech House, Boston, 1993).
[18] It is this stochastic nature of the Monte Carlo simulation method that provides its name, a reference to the gambling opportunities in the eponymous Mediterranean city.
[19] M. A. Green, J. Appl. Phys. **67**, 2944 (1990).
[20] D. Long, Phys. Rev. **120**, 2024 (1960).
[21] C. Hamaguchi, *Basic semiconductor physics* (Springer, New York, 2001).
[22] C Herring and E. Vogt, Phys. Rev. **101**, 944 (1956).
[23] A. Haug, *Theoretical solid state physics* (Pergamon Press, New York, 1972), Vol. 2.
[24] H. Mizuno, K. Taniguchi, and C. Hamaguchi, Phys. Rev. B **48**, 1512 (1993).
[25] M. V. Fischetti and S. E. Laux, J. Appl. Phys. **80**, 2234 (1996).
[26] M. V. Fischetti and S. E. Laux, Phys. Rev. B **48**, 2244 (1993).
[27] P. Y. Yu and M. Cardona, *Fundamentals of Semiconductors* (Springer, New York, 1996).
[28] E. Sangiorgi, B. Ricco, and F. Venturi, IEEE Trans. Comput.-Aided Des. **7**, 259 (1988).
[29] E. Pop, Master's thesis, M. I. T., 1999.
[30] K. Ismail, S. Nelson, J. Chu, and B. Meyerson, Appl. Phys. Lett. **63**, 660 (1993).
[31] S. Nelson, K. Ismail, J. Chu, and B. Meyerson, Appl. Phys. Lett. **63**, 367 (1993).
[32] M. M. Rieger and P. Vogl, Phys. Rev. B **48**, 14276 (1993).
[33] Good agreement with the theoretical results was serendipitous, as the current empirical set of deformation potentials had already been settled upon when the results of the *ab initio* calculations came to our attention.
[34] S. Sinha, E. Pop, and K. E. Goodson, in Int. Mechanical Engineering Congress and Exp. (Anoheim CA, November 2004).
[35] Monet, available in http://nanoheat.stanford.edu
[36] M. H. Joegensen, Phys. Rev. B **18**, 5657 (1978).
[37] G. Dolling, in *Symposium on Inelastic Scattering of Neutrons in Solid and Liquids* Vol. 2, (IAEA, Chalkriver, 1963) pp. 37–48.